NANO LETTERS

Letter

pubs.acs.org/NanoLett

Label-Free Detection of Single Protein Using a Nanoplasmonic-Photonic Hybrid Microcavity

Venkata R. Dantham,[†] Stephen Holler,[†,‡] Curtis Barbre,[†] David Keng,[†] Vasily Kolchenko,[§] and Stephen Arnold[†,*]

[†]Microparticle Photophysics Lab, Polytechnic Institute of NYU, Brooklyn, New York 11201, United States

[‡]Department of Physics, Fordham University, Bronx, New York 10458, United States

[§]Department of Biological Sciences, NYC College of Technology, Brooklyn, New York 11201, United States

ABSTRACT: Recently we reported the detection and sizing of the smallest RNA virus MS2 with a mass of 6 ag from the resonance frequency shift of a whispering gallery mode-nanoshell hybrid resonator (WGM-h) upon adsorption on the nanoshell and anticipated that single protein above 0.4 ag should be detectable but with considerably smaller signals. Here, we report the detection of single thyroid cancer marker (Thyroglobulin, Tg) and bovine serum albumin (BSA) proteins with masses of only 1 ag and 0.11 ag (66 kDa), respectively. However, the wavelength shifts are enhanced beyond those anticipated in our earlier work by 240% for Tg and 1500% for BSA. This surprising sensitivity is traced to a short-range reactive field near the surface of our Au nanoshell receptor due to intrinsic random bumps of protein size, leading to an unanticipated increase in sensitivity to single protein, which grows larger as the protein diminishes in size. As a consequence of the largest signal-to-noise ratio in our BSA experiments ($S/N \approx 13$), we conservatively estimated a new protein limit of detection for our WGM-h of 5 kDa.

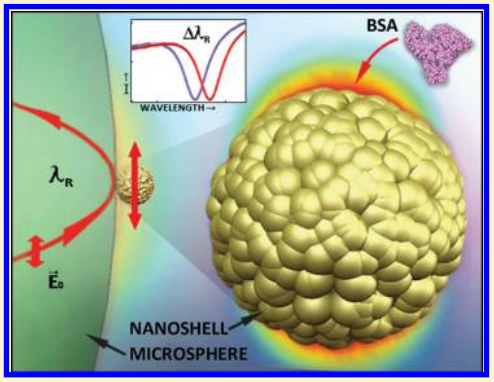

KEYWORDS: *Whispering gallery mode, hybrid microcavity, surface plasmons, single protein detection, BSA protein, label-free detection, nanoshell, thyroid cancer marker*

Single protein (molecule) detection provides rich and critical molecular information in fundamental biochemical research and biomedical applications.[1,2] Traditionally, single molecule detection relies primarily on fluorescence microscopy, which requires sophisticated instruments and complicated dye-labeling processes that may adversely affect a molecule's functionality.[3,4] In contrast to this, label-free detection of single bionanoparticles (e.g., virus, protein) allows these particles to be detected in their native state (i.e., without interference from fluorescent labels)[5,6] with interactions potentially able to be followed in real time.[7] Size/mass information can be extracted from the measured signals. In 2010, Mayer et al[8] identified single IgG antigen (molecular weight 150−160 kDa) unbinding events in a statistical way (signal-to-noise ratio, $S/N \sim 1$) from the antibodies anchored to a gold bipyramid. In 2012, Ament et al[9] demonstrated the detection of a larger protein Fibronectine (450 kDa) in real time using a nanorod with a S/N not exceeding ~4. A major difficulty was that the line width ($\delta\lambda_R \sim$ 50 nm) of the localized surface plasmon resonance (LSPR) was considerably larger than the average shift ($\Delta\lambda_R \sim 0.3$ nm). Later, Zijlstra et al.[10] demonstrated the detection of smaller single proteins (Streptavidin, 53 kDa) by adsorbing to a gold nanorod using a photothermal microscope technique with $S/N \sim 1.5$. This technique required a great deal of free-space optics, and it is difficult to see how it can be easily multiplexed.

Alternatively, an optical WGM microcavity driven by waveguide allows the label-free detection of bionanoparticles in an all photonic fashion and can be generated by lithography.[5,6,11] Detection is mainly based on monitoring the change in free space resonance wavelength (wavelength shift, $\Delta\lambda_R$) upon adsorbing a bionanoparticle to the microcavity. However, detection and sizing of the smallest bionanoparticles one at a time using bare microcavities has been frustrated for lack of sufficient sensitivity.[12] Consequently, the bare microcavity approach has given way to hybrid microcavities using nanoplasmonic-enhancing-epitopes.[13] A typical resonance line width of the hybrid microcavity is easily one hundred thousand times smaller than the width of a LSPR, thereby affording the WGM-h with a distinct advantage.

Recently we reported the detection and sizing of the smallest RNA virus MS2 with a mass of 6 ag[14] by constructing a hybrid microcavity with a single gold nanoshell attached to the equator of a microspherical dielectric resonator operating in a WGM.[15] By driving this WGM-h near the nanoshell's dipole plasmon resonance, wavelength shift steps were observed upon the adsorption of MS2 to the surface of the nanoshell which were

Received: May 4, 2013
Revised: June 17, 2013
Published: June 18, 2013

 © 2013 American Chemical Society dx.doi.org/10.1021/nl401633y | *Nano Lett.* 2013, 13, 3347−3351

enhanced by 70× beyond those of the bare microcavity, thereby allowing the virus to be detected and sized (27 nm diameter) based on the assumption of a smooth shell surface. Although subattogram single protein detection was anticipated, the signals should have challenged our existing limit of detection (LOD) of 0.4 ag.[14] Here we report the detection of single thyroid cancer marker (Thyroglobulin, Tg) and bovine serum albumin (BSA) proteins with masses only 1 and 0.11 ag (66 kDa), respectively. However, the wavelenth shifts are enhanced beyond those anticipated in our earlier work by 240% for Tg and 1500% for BSA. This surprising sensitivity is traced to a short-range reactive field near the surface of our Au nanoshell receptor due to intrinsic random bumps[16−19] with heights (4−10 nm) comparable to a protein size (Figure 1). The overlap between these short-range reactive fields and a single protein adsorbing to a bump leads to the unanticipated increase in sensitivity.[20] In what follows, we will describe our WGM-h and protein sample preparation, construct a model for understanding such an enhancement mechanism, and present data demonstrating single protein detection that utilizes this mechanism.

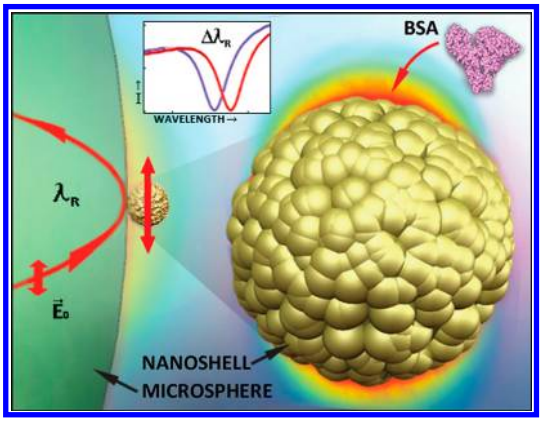

Figure 1. Illustration of a BSA protein adsorbing at the surface of a bump on a nanoshell, attached to a dielectric microcavity. The effective overlap between the enhanced near field intensity of a bump decorated nanoshell and a protein dielectric profile leads to enhancement in WGM-h wavelength shift upon adsorption that is well beyond that expected from a smooth shell attached to the same microcavity.

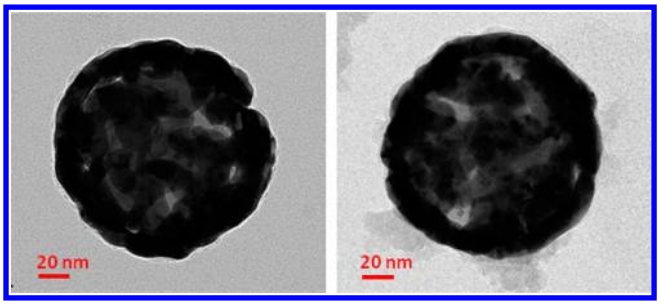

Figure 2. TEM images of silica core-gold nanoshells.

Our hybrid microcavity consists of a gold nanoshell assembled by light-forces to the equator of slightly oblate silica microsphere supporting a traveling WGM with transverse electric (TE) polarization. The schematic of our experimental setup and method for attaching a single gold nanoshell to a microcavity can be found elsewhere.[14] In brief the WGM-h and a tapered fiber contacting the resonator are embedded in a microfluidic polydimethyl siloxane (PDMS) channel. A guided wave in the fiber generated by a tunable distributed feedback laser evanescently drives the resonator near 780 nm. In order to

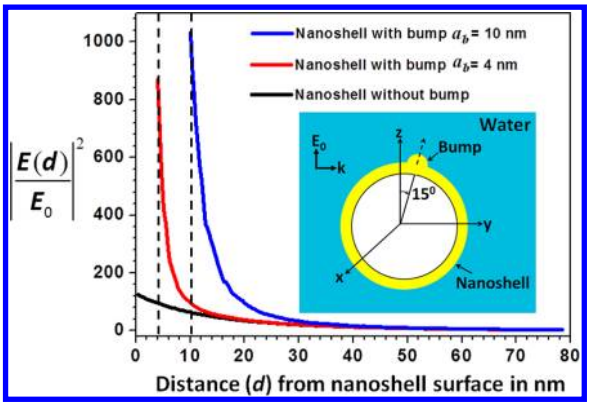

Figure 3. Enhancement in intensity just above hemispherical bumps of different radii (a_b) on a gold nanoshell (inner radius r_1 = 60 nm and outer radius r_2 = 71.5 nm) at the dipole resonance of the nanoshell at 780 nm (blue and red) and enhancement above the smooth nanoshell (black). All separations d are measured from the nanoshell surface along the dashed line (---) shown in inset.

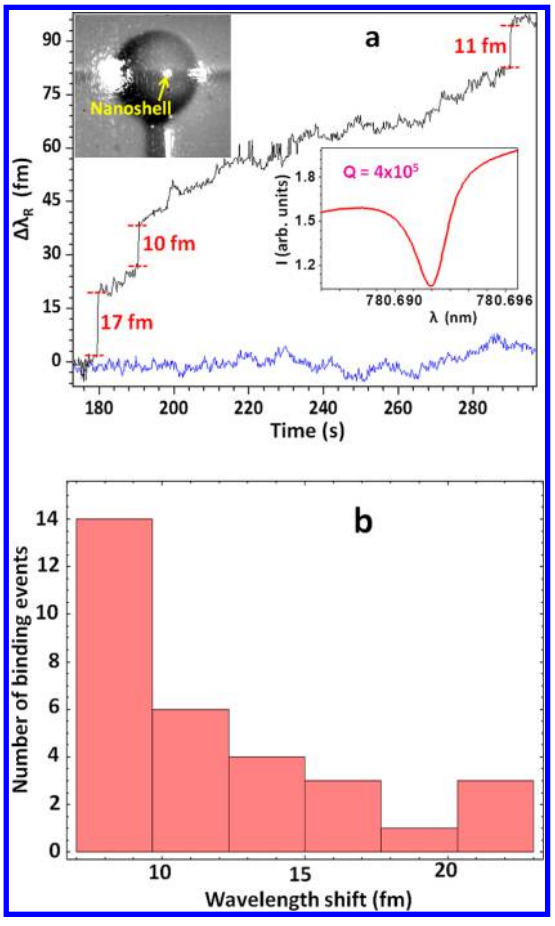

Figure 4. (a) Resonance wavelength shift curve (upper) shows steps associated with single Tg protein adsorbing to the gold nanoshell attached at the equator of WGM resonator with $R \sim 35$ μm. Insets show a microscopic image of the WGM-h and its resonance spectrum. The lower trace shows the background without protein or the gold nanoshell (rms noise ~ 1 fm). Points were taken 1/5 s apart while maintaining a bandwidth of ~10^3 Hz. (b) The combined step number statistics obtained from two experiments on these proteins.

dx.doi.org/10.1021/nl401633y | Nano Lett. 2013, 13, 3347−3351

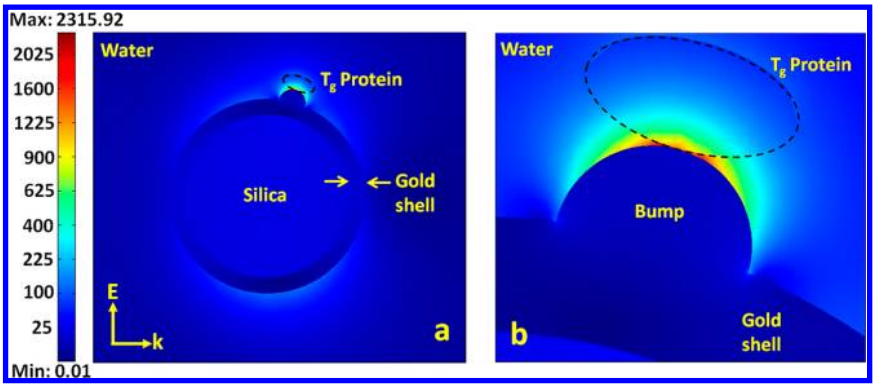

Figure 5. (a) FEM simulation of the parking of Tg protein at a bump of radius 10 nm on the surface of a nanoshell with r_1 = 60 nm and r_2 = 71.5 nm. The field intensity at the interface between the bump and protein rises to 2315× the incident field as indicated by the rainbow scale on the left. (b) The magnified image of the protein on the bump.

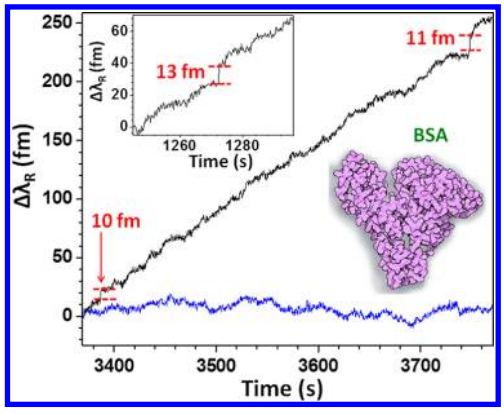

Figure 6. Resonance wavelength shift curve (upper) shows steps associated with single BSA protein adsorbing to the gold nanoshell attached at the equator of WGM resonator $R \sim 32$ μm. Insets show the maximum step associated with this protein and the spacing filling model of BSA protein. The lower trace shows the background without protein or the gold nanoshell (rms noise ~ 1 fm). Points were taken 1/5 s apart while maintaining a bandwidth of ~10^3 Hz.

avoid nonlinear effects the power injected into the fiber is low, 50 μW.

Tg and ultra pure BSA were obtained from Sigma Aldrich (product no. T1001) and Ambion (cat. no. 2618), respectively. At constant temperature and pH, the rate of aggregation mainly depends upon the initial monomeric concentration.[21−23] Therefore it can be controlled by reducing the concentration of the sample. So far researchers have reported aggregation effects at larger protein concentrations (>1 mg/mL).[21,22] We prepared protein solutions in deionized water with the concentration of 300 fM (~0.2 ng/mL). Therefore, the probability of forming aggregates is substantially lower in our solutions. It is to be noted that our concentration was 10^6 times lower than that used in the previous single protein detection experiment.[10] The mean isoelectric point of Tg and BSA are 4.5 and 4.7, respectively. This leads to negative charge on their surface in water at our pH ~ 7. Since our gold nanoshell has negative charge on its surface, these proteins are repelled from the nanoshell's surface unless there are strong attractive light forces.[7,13,24,25] To aid these forces, the microfluidic channel[14] is brought to a salt (NaCl) concentration of 30 mM to increase the conductivity of the solution and thereby reduce the range of the electrostatic fields emanating from the silica−water and gold−water interfaces.

The basis for our model associated with enhancement beyond what is possible from a smooth nanoshell is motivated by the actual character of the gold surface. Gold nanoshells (Nano Spectra Biosciences) obtain a rough nature due to synthesis from colloidal gold nanoparticles that are added to the surface of a silica nanosphere. The nanoshells used in our experiments have an average shell thickness of ~11.5 nm from spectroscopic data[14] and were further characterized by transmission electron microscopy (TEM). As Figure 2 shows, although a typical nanoshell has nominal diameter of ~143 nm

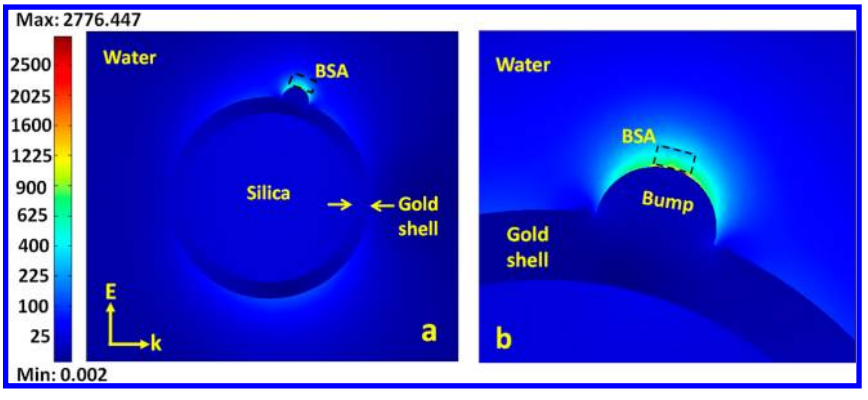

Figure 7. (a) FEM simulation of the parking of BSA protein at a bump on the surface of a plasmonic nanoshell with r_1 = 60 nm and r_2 = 71.5 nm. The field intensity at the position of the protein rises to 2776× the incident field as indicated by the rainbow scale on the left. (b) The magnified image of the protein on the bump.

dx.doi.org/10.1021/nl401633y | Nano Lett. 2013, 13, 3347−3351

they are covered with distinct bumps having heights ranging from 4 to 10 nm. The effect which such bumps have on the far and near field of a nanoshell has been investigated over the past decade.[16−19]

Oubre and Norlander theoretically predicted that these random bumps hardly influence the LSPR wavelength of a nanoshell.[26] Modification of electrical field intensity at the surface of a nanoshell in the presence of several random bumps was investigated using finite element method (FEM) to understand the averaged surface enhanced Raman scattering (SERS) signal of several molecules adsorbed to that nanoshell.[18] The expected SERS signal strength was proportional to the surface integrated quadratic field of a nanoshell ($\int |E|^4 ds$) and was enhanced by a small factor (∼4) due to the random bumps. Talley et al.[18] pointed out that the largest contribution to the surface average SERS signal should be associated with adsorption on convex nanobumps. In what follows, we will show in an elemental way that this insight also leads to a mechanism for added enhancement of a WGM-h resonator, allowing single protein to be detected by such a device for the first time.

Unlike SERS the expected WGM wavelength shift signal due to the single protein adsorption events mainly depends on the intensity ($|E|^2$) at the surface of that bump. Therefore, FEM simulations (Comsol) were carried out to investigate the enhancement just above a bump located at the highest intensity point of a "smooth" shell. For our shells, the highest intensity point at 780 nm (dipole resonance) occurs in the forward direction by 15°. Consequently, we have placed a bump at this location in order to estimate the maximum local field enhancement (Figure 3). As can be seen, for 4 and 10 nm radius bumps on a nanoshell (silica core radius r_1 = 60 nm and shell radius r_2 = 71.5 nm) the intensity enhancement increases by ∼700% and ∼840%, respectively, at the surface of the bump in comparison with the smooth-shell.

Now the major question is: how large is the influence on the WGM wavelength shift signal due to the enhanced local field on the bump surface? This can be answered based on the reactive sensing principle (RSP)[7,27,28] for which a wavelength shift $\Delta\lambda_R$ smaller than the resonance line width is proportional to the excess polarization energy of the analyte. Therefore, the enhancement in wavelength shift (ξ) as represented by the ratio of the shift due to adsorption on the nanoshell epitope to that just outside a bare portion of the microcavity equator is

$$\xi = \frac{(\Delta\lambda_R)_{\text{withshell}}}{(\Delta\lambda_R)_{\text{withoutshell}}} = \frac{\int \Delta\varepsilon (E_b \cdot E_a^*)_{\text{withshell}}\, dV_{\text{analyte}}}{\int \Delta\varepsilon (E_b \cdot E_a^*)_{\text{withoutshell}}\, dV_{\text{analyte}}} \quad (1)$$

where $\Delta\varepsilon = \varepsilon_d - \varepsilon_m$, ε_d is the relative permittivity of the analyte, ε_m is the permittivity of the medium, $E_b \cdot E_a^*$ is the product of the field before the analyte insertion with that after the analyte insertion, and V_{analyte} is the volume of the analyte. Since this shift is referenced to one and the same underlying high quality (Q) bare microcavity, ξ is independent of losses.[14,15] The numerator of the eq 1 depends upon the overlap between localized near field intensity of the bump and the form of the adsorbed analyte. Since the bump radius a_b is on the order of a protein size (∼5 nm), and the local intensity a distance s above the bump drops off roughly as $\sim[a_b/(a_b + s)]^6$, there is effective overlap between the near field intensity of a bump and a protein dielectric profile. However, the local field at the bump hardly influences the wavelength shift signal due to virus particles, since they are considerably larger. We have verified through FEM simulations that the smallest virus (MS2) has its wavelength shift signal increased by only 25% beyond the effect of a smooth nanoshell enhancement upon adsorption to a 10 nm bump. Since the wavelength shift is proportional to the cube of the viral radius,[14] no more than a 8% error results in the size, which explains why the enhancement due to roughness was not apparent in our previous experiment on MS2.[14] In what follows, we present the experimental data on the Tg thyroid cancer marker.

Before recording dip trace characteristics of the WGM-h, we adsorbed Tg protein onto a bare microcavity. A wavelength shift binding curve was recorded characteristic of nonspecific adsorption with no detectable steps. Next, we carried out the same experiment with a WGM-h of radius $R \sim 35$ μm. A portion of a typical dip trace is displayed in the upper curve in Figure 4a. The clear steps indicate the adsorption of single Tg proteins on the nanoshell with the gradually increasing background due to adsorption of protein on the silica surface. Step heights were quantified by using a derivative algorithm.[29] The wavelength step height statistics accumulated from two different experiments are shown in Figure 4b. A total of 40 steps were recorded over 4000 s in the two experiments with a maximum step height of 22 femtometers (fm). Adsorption of individual protein at the equator of the bare microcavity of the same radius produces a theoretical shift[27] of ∼0.06 fm, which is well below the RMS noise (1 fm). Using eq 1, the expected shift for the single protein adsorption to a smooth-shell attached to the microcavity (R = 35 μm) is ∼6.5 fm with enhancement in wavelength shift $\xi_{\text{smooth shell}}$ ∼108, below the maximum measured step height of 22 fm, by factor ∼3. This clearly indicates an additional enhancement for which a roughness hypothesis associated with bumps will be shown to be both reasonable and unavoidable.

To investigate the influence of a bump on the wavelength shift, FEM simulations were carried out for a single protein adsorbed to a bump on the nanoshell using eq 1. Figure 5a shows the result at 780 nm for a model Tg protein[30] (prolate spheroid, semimajor axis 11 nm, radius 5.5 nm, refractive index 1.5) adsorbed to a bump of radius 10 nm at the highest intensity point on a nanoshell with r_1 = 60 nm and r_2 = 71.5 nm. It can be seen that the intensity at the bump surface is distinctly enhanced relative to the nanoshell surface with a calculated wavelength shift enhancement $\xi_{\text{bump}} \sim 245$. On this basis, two-thirds of the experimental enhancement is explained, and a lot larger enhancement is anticipated by generating a larger overlap between a smaller protein profile and the same bump intensity. In what follows, we present experimental data on a much smaller protein.

A further experimental rationale for attempting to detect a smaller protein is that the S/N in the Tg experiments was high (22:1). With extreme care to avoid protein clusters as described earlier we next looked at BSA which has a mass one tenth that of Tg. As a control, a wavelength shift binding curve was recorded using a bare cavity with $R \sim 32$ μm, which resulted in a characteristic nonspecific binding curve with no detectable steps. Next, we carried out the same experiment with a WGM-h for which the dielectric microsphere had a similar radius to that in the control experiment. Clear steps associated with BSA protein were recorded as shown in Figure 6 (upper curve). A total of 22 steps were recorded over 5000 s in two experiments with step heights ranging from 7 to 13 fm (shown in inset of Figure 6). Adsorption of individual BSA protein at the equator

dx.doi.org/10.1021/nl401633y | Nano Lett. 2013, 13, 3347−3351

of the bare microcavity of the same radius produces a theoretical shift[27] ~0.006 fm. Using eq 1, the expected shift for the single protein adsorption to a smooth-shell attached to the microcavity of same radius is ~0.8 fm ($\xi_{\text{smooth shell}}$ = 138). This clearly indicates that the bumps effectively influence the wavelength shift signal. FEM simulations were carried out on BSA protein adsorbed at a bump (a_b = 10 nm). Figure 7a shows the result at 780 nm for a model BSA protein[27,31] (short cylinder diameter 6.8 nm, height 3.4 nm, refractive index 1.5) adsorbed to a bump at the highest intensity point on a nanoshell.

The value of ξ_{bump} obtained from this simulation is ~635 as compared with ~245 for Tg. Therefore, BSA protein adsorbed on a 10 nm bump produces theoretical shift 635 × 0.006~4 fm, which agrees well with our smaller observed steps in the BSA experiment.

In conclusion, we have successfully demonstrated the detection of single Tg and BSA proteins using our hybrid microcavity. The signal-to-noise ratios in the experimental results associated with these proteins are 22:1 and 13:1, respectively. From the *S*/*N* in the BSA experiment we conservatively estimate the protein limit of detection (LOD) in our WGM-h to be the mass of BSA divided by 13, or ~0.008 ag (5 kDa). Consequently, it should be easy to detect single protein markers of various dangerous cancers such as breast cancer (290 kDa), lung cancer (176 kDa), liver cancer (70 kDa), and melanoma (84 kDa).

AUTHOR INFORMATION

Corresponding Author

*E-mail: sarnold935@aol.com.

Notes

The authors declare no competing financial interest.

ACKNOWLEDGMENTS

The authors thank the National Science Foundation (NSF) for supporting this work (Grant CBET 0933531).

REFERENCES

(1) Zander, C.; Enderlein, J.; Keller, R. A. *Single-molecule detection in solution: Methods and applications*; Wiley-VCH: Hoboken, NJ, 2002.

(2) Leuba, S. H.; Zlatanova, J. *Biology at the Single Molecule Level*; Pergamon Press: New York, 2001.

(3) Moerner, W. E.; Fromm, D. P. *Rev. Sci. Instrum.* **2003**, *74* (8), 3597−3619.

(4) Gell, C.; Brockwell, D.; Smith, A. *Handbook of single molecule fluorescence spectroscopy*; Oxford University Press: Oxford, 2006.

(5) Luchansky, M. S.; Bailey, R. C. *Anal. Chem.* **2012**, *84*, 793−821.

(6) Sun, Y.; Fan, X. *Anal. Bioanal. Chem.* **2011**, *399* (1), 205−211.

(7) Arnold, S.; Keng, D.; Shopova, S. I.; Holler, S.; Zurawsky, W.; Vollmer, F. *Opt. Express* **2009**, *17* (8), 6230−6238.

(8) Mayer, K. M; Hao, F.; Lee, S.; Nordlander, P.; Hafner, J. H. *Nanotechnology* **2010**, *21*, 255503.

(9) Ament, I.; Prasad, K.; Henkel, A.; Schmachtel, S.; Sönnichsen, C. *Nano Lett.* **2012**, *12* (2), 1092−1095.

(10) Zijlstra, P.; Paulo, P. M. R.; Orrit, M. *Nat. Nanotechnol.* **2012**, *7* (6), 379−382.

(11) Chamanzar, M.; Adibi, A. *Opt. Express* **2011**, *19* (22), 22292−22304.

(12) Arnold, S.; Ramjit, R.; Keng, D.; Kolchenko, V.; Teraoka, I. *Faraday Discuss.* **2007**, *137*, 65−83 (discussion pp 99−113).

(13) Arnold, S.; Dantham, V. R.; Barbre, C.; Garetz, B. A.; Fan, X. D. *Opt. Express* **2012**, *20* (24), 26147−26159.

(14) Dantham, V. R.; Holler, S.; Kolchenko, V.; Wan, Z.; Arnold, S. *Appl. Phys. Lett.* **2012**, *101* (4), 043704.

(15) Shopova, S. I.; Rajmangal, R.; Holler, S.; Arnold, S. *Appl. Phys. Lett.* **2011**, *98* (24), 243104.

(16) Oldenburg, S. J.; Westcott, S. L.; Averitt, R. D.; Halas, N. J. *J. Chem. Phys.* **1999**, *111* (10), 4729−4735.

(17) Jackson, J. B.; Halas, N. J. *Proc. Natl. Acad. Sci U.S.A.*. **2004**, *101* (52), 17930−17935.

(18) Talley, C.; Jackson, J. B.; Oubre, C.; Grady, N. K.; Hollars, C. W.; Lane, S. M.; Huser, T. R.; Nordlander, P.; Halas, N. J. *Nano Lett.* **2005**, *5* (8), 1569−1574.

(19) Wang, H.; Goodrich, G. P.; Tam, F.; Oubre, C.; Nordlander, P.; Halas, N. J. *J. Phys. Chem. B* **2005**, *109*, 11083−11087.

(20) Laor, U.; Schatz, G. C. *J. Chem. Phys.* **1982**, *76* (6), 2888−2899.

(21) Shire, S. J.; Shahrokh, Z.; Liu, J. *J. Pharm. Sci.* **2004**, *93* (6), 1390−1402.

(22) Fink, A. L. *Folding Design* **1998**, *3* (1), R9−R23.

(23) Roefs, S. P. F. M.; Kruif, K. G. D. *Eur. J. Biochem.* **1994**, *226*, 883−889.

(24) Novotny, L.; Bian, R. X.; Xie, X. S. *Phys. Rev. Lett.* **1997**, *79* (4), 645−648.

(25) Ahn, W.; Boriskina, S. V.; Hong, Y.; Reinhard, B. M. *ACS Nano* **2012**, *6* (1), 951−960.

(26) Oubre, C.; Nordlander, P. *J. Phys. Chem. B* **2004**, *108*, 17740−17747.

(27) Arnold, S.; Khoshsima, M.; Teraoka, I.; Holler, S.; Vollmer, F. *Opt. Lett.* **2003**, *24* (4), 272−274.

(28) Teraoka, I.; Arnold, S. *J. Opt. Soc. Am. B* **2006**, *23* (7), 1381−1389.

(29) Dantham, V. R.; Holler, S.; Kolchenko, V.; Wan, Z.; Arnold, S. *Proc. SPIE* **2013**, *8600*, 86001P−1−86001P-6.

(30) Bloth, B.; Bergquist, R. *J. Exp. Med.* **1968**, *128*, 1129.

(31) Carter, D. C.; He, X.-M.; Munson, S. H.; Twigg, P. D.; Gernert, K. M.; Broom, M. B.; Miller, T. Y. *Science* **1989**, *244*, 1195−1198.